

ANTIMONY RECOVERY FROM RECYCLED TERMINALS OF LEAD-ACID BATTERIES WITH Na_2CO_3 AND SiC AFTER THE FORMATION OF Sb_2O_3

J.C. Jiménez-Lugos ^a, R.G. Sánchez-Alvarado ^a, A. Cruz-Ramírez ^{a,*},
J.A. Romero-Serrano ^a, A. Hernández-Ramírez ^a, J.E. Rivera-Salinas ^b

^a Instituto Politécnico Nacional - ESQIE, Departamento de Ingeniería en Metalurgia y Materiales, Ciudad de México, México

^b Centro de Investigación en Química Aplicada - CIQA, Department of Plastics Transformation Processing, Saltillo, Coahuila, México

(Received 16 June 2021; accepted 04 November 2021)

Abstract

Terminals obtained from spent lead-acid batteries in Mexico contain around 2 wt% Sb. The terminals were melted in an electric furnace and then oxygen was injected at 750 °C with a gas flow rate of 2 L/min to produce high purity Sb_2O_3 . The antimony trioxide obtained was treated with a mixture of Na_2CO_3 -SiC at 1000 °C to obtain metallic antimony. The antimony trioxide was reduced by C present in reagents while silicon and sodium formed a slag phase. The amounts of Sb_2O_3 and SiC were held constant while the Na_2CO_3 was evaluated in the range from 30 to 42 wt%. The produced antimony and slag were characterized by the X-ray diffraction and SEM-EDS techniques. The addition of 34 wt% Na_2CO_3 led to the recovery of antimony up to 90.16 wt% (99.57 wt% purity) and the lowest antimony losses in the slag (2 wt%). In addition, the compounds Na_2SiO_3 and $\text{Na}_2\text{Si}_2\text{O}_7$ formed in the slag indicated a more stable slag. Na_2CO_3 contents higher than 38 wt% decreased the antimony recovery since $\text{Na}_2\text{Sb}_4\text{O}_7$ compound was promoted in the slag. The oxidation and reduction process was modeled in FactSage 7.3 software for a better understanding of the Na_2CO_3 and SiC additions on the antimony recovery rates and compounds formed in the slag.

Keywords: Antimony; Reduction; Slag; Batteries; Thermodynamic

1. Introduction

Various unique properties of antimony determine its use in a diverse range of products and applications. Some of these properties include low melting point, enhancing workability at low temperatures, stability in the air at room temperature and in water to 250 °C, resistance to most cold acids, dissolution in some hot acids and aqua regia, high density (6,692 kg/m³), low electrical and thermal conductivity, and expansion on freezing, like silicon bismuth gallium, and germanium [1]. Antimony is a metal that has had through decades different uses, and the most important applications of antimony are in the production of flame retardants, PET catalysis, ceramics, and glass [2, 3]. Antimony is also widely used in metallic form in alloys and compounds, in lead alloys such as grids and terminals in lead-acid batteries to increase their hardness [4-7], and antimony bearing alloys (babbitts) which contain 4-5% of antimony for high anti-friction properties, low coefficient of friction in the bearings, and good

conformability [8], as compounds with As, Ga, and In, antimony is also used for camouflage paints production [5]. Other uses of antimony as oxides or sulfides are in pigments and red rubber in vulcanizing applications [5, 7]. After its use, once the end life cycle of those antimony-bearing products is completed, they are subject to disposing, recycling, or landfilling. Antimony content in products that reached their end life cycle is crucial to define if they can be considered as waste, reusable materials or if they can be treated in a recycling process for its recovery. Some products such as lead grids and terminals in lead-acid batteries are considered as a secondary source of antimony since they contain between 1.6 and 7% antimony [9, 10], the by-product from lead-smelting called antimonial dust also represents an important secondary resource. In the pyrometallurgical process for antimonial dust reduction, the reverberatory furnace is used to enrich its concentration in the intermediate product of crude lead-antimony alloy, then the resulting alloy should be

*Corresponding author: alacruzr@ipn.mx



converted and reduced several times until white antimony products quality is reached [11]. Z. Da-peng et al. [12] recovered antimony from antimony-bearing dust through a reduction-roasting process. First, the dust was roasted and then a CO-CO₂ mixture was used as a reducing agent. The antimony recovery was in the range from 66 to 73.81 wt% when the temperature was increased from 650 to 800 °C, respectively. On the other hand, the main primary antimony production starts with the processing of mineral Stibnite (Sb₂S₃) which is an abundant antimony bearing mineral, and thus it is the main source for production of pure antimony trioxide and/or metallic antimony [13]. The conventional technology to produce metallic antimony from stibnite concentrates is primarily by oxidizing roasting to convert the stibnite into volatile antimony oxide (Sb₂O₃), which is subsequently reduced to antimony metal with carbon [14]. In pyrometallurgical antimony production, which is done in equipment such as the shaft furnace, rotary kiln, converter, or reverberatory furnace, a considerable amount of slag containing antimony and other impurities is formed. The amount of waste slag produced for each ton of antimony is about 5 tons. Slag waste is partially reused in the pyrometallurgical process to diminish antimony volatilization [3], nonetheless, in most cases, the desired recoveries and grades for antimony are not obtained in a single step process. The pyrometallurgical process for refining lead bullion includes the oxidation refining process and basic refining process, which both are based on the principle that antimony is oxidized more easily than lead therefore alloys containing lead and antimony can be separated pyrometallurgically, due to their vapor pressure difference [15]. J. Xu et al. [16] determined the activities of the components of Pb-Sn-Sb ternary alloy by equilibrium test to 2 Pa and temperatures in the range from 1023 to 1223 K. The experimental vapor-liquid equilibria data of the ternary alloy was calculated with the Wilson equation and predicted values matched reasonably with the experimental results. The proposed study was of great significance to the experimental design that involved vacuum distillation processes, specifically for the Pb-Sb-Sn recycling alloys. Z. T. Zhang et al. [17] studied the antimony distribution of SiO₂ saturated Sb-Fe-O-SiO₂-CaO system by high-temperature experiments and quenching techniques. The ratios Fe/SiO₂ and CaO/SiO₂ on the Sb₂O₃ content were evaluated to 1200 °C for the proposed system. The phases contained in the slag were analyzed by the X-ray diffraction and SEM-EDS techniques to 900 and 1200 °C. Higher antimony recoveries were obtained beyond 94 % which indicated the reduction of antimony content in the slag. Either from slags in primary antimony production or secondary antimony resources like by-products from lead-smelting,

antimony is present or recovered mainly as antimony trioxide where metallic antimony can be reclaimed. Besides, some attractive alternatives have been proposed for antimony and lead recovery through the hydro/electro-metallurgy route. J.A. Barragan et al. [18] recovered Sb and Cu from electronic waste through hydro/electro-metallurgical technics, copper was recovered as the main component in a leaching solution, whereas the antimony (as Sb₂O₃ with commercial quality) recovery process was established as a purification step, achieving a rate of 81 wt.-%, while in [19] they calculated the values of potential (E vs NHE) and pH at which the leaching reactions occurred spontaneously, as well as the deduction of a quadratic semiempirical model to predicts the copper, lead and silver leaching efficiencies as a function of the stirring speed and the solid/liquid ratio, optimizing the leaching efficiency. Because of the growing recycling volume of lead-acid batteries in Mexico and the high lead and antimony content in the terminals of the battery, it is necessary to develop new routes for antimony recovery that allow maximum recovery and grade through a practical processing route. Taking these requirements into account, the pyrometallurgical route appears to be more suitable in the recovery of antimony from the recycling of lead acid battery terminals. Mixtures of Na₂CO₃ and SiC were used successfully for the lead paste reduction obtained from the recycling of lead-acid batteries by a pyrometallurgical route where a high lead recovery was obtained [20]. Thus, SiC was chosen as a reducing agent instead of traditionally used carbon for the antimony oxides reduction, with the advantage at the same time of both, the possibility of the formation of a stable slag based on silicates structures and to provide carbon as a reducing agent of antimony oxides. The aim of this work is focused on the antimony recovery from the terminals obtained from spent lead-acid batteries by an oxidation-reduction process. Oxygen was injected through a lance to the antimony volatilization and then the trioxide antimony was recovered which was reduced by a mixture of Na₂CO₃ and SiC to produce technical grade antimony. The obtained products (slag and antimony button) were analyzed by the X-ray diffraction and SEM-EDS techniques. The pyrometallurgical process was thermodynamically modeled in FactSage 7.3 [21] and the predicted results matched the experimental phases obtained and the antimony recovery rates.

2. Experimental Procedures

2.1. Pb-Sb alloy

Terminals were obtained from spent lead-acid batteries and melted in an electric furnace at 400 °C. The lead-antimony alloy was poured into a pre-heated



iron mold and sampled for chemical analysis.

2.2. Oxidation stage

The antimony volatilization from the Pb-Sb alloy was carried out with the scheme depicted in Figure 1.

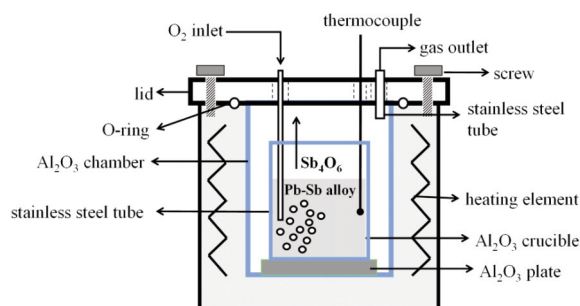


Figure 1. Experimental array for the antimony volatilization

500 g of the Pb-Sb alloy were charged into an alumina crucible contained in an alumina chamber inside an electric furnace enabled with control of temperature within ± 10 °C of the set values. The alumina chamber was tightly sealed by a stainless-steel lid, screws, and a high-temperature o-ring located on the inner side of the lid. The stainless-steel lid contained two inlets and one outlet. The inlets contained two stainless steel tube that allowed the oxygen injection and the temperature measurement by a k-type thermocouple, while the outlet allowed the gas exhaust which was conducted to a water jacket-cooled glass vessel. The furnace temperature control was set up at 750 °C and when the inner temperature equaled the programmed temperature, oxygen (99.5 wt% purity) was injected through a stainless-steel tube into the melted alloy at a rate of 2 liters per minute over 35 seconds (about 1.5 grams O_2). After oxygen injection, the furnace was switched off and it was left to be cooled. The collected powder was weighed and analyzed by the X-ray powder diffraction and atomic absorption techniques.

2.3. Reduction stage

The reduction stage was carried out using commercial reagents of Na_2CO_3 and Sb_2O_3 in powder form with ≥ 99.5 and 99.9 wt% of purity, respectively. High purity (≥ 99 wt%) spent SiC crucibles were used with a mean particle size of 74-125 microns. Four trials were carried out to attain constant amounts of Sb_2O_3 and SiC in 5 and 0.95 g, respectively, while the Na_2CO_3 was set to 2.5, 3.1, 3.7, and 4.3 g which correspond to 30, 34, 38, and 42 wt%, respectively. The reagents for each trial were weighted in a Sartorius TE64 Talent Analytical Balance, 60 g x 0.1 mg readability, and mixed thoroughly in an agate

mortar. The mixtures were charged in alumina crucibles with a capacity of 20 mL, the crucibles were covered with alumina lids. The covered alumina crucibles with the corresponding mixed reagents for each trial were placed in an electrical resistance furnace with control of temperature to within ± 10 °C, each experiment lasted 1 hour to 1000 °C. The temperature was also measured with a type k thermocouple. The experimental setup for antimony oxide reduction with Na_2CO_3 and SiC is shown in Figure 2.

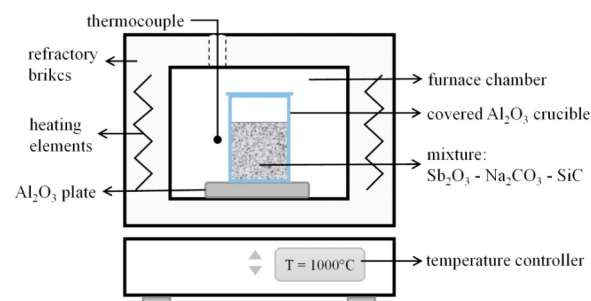


Figure 2. Experimental set up for antimony oxide reduction

After the reaction time, the furnace was turned off. The smelted products (metal and slag) were poured and cooled down in an iron mold. Metallic antimony and slag were separated, weighed, and analyzed by the X-Ray Diffraction, Absorption Atomic Spectrometry, and Scanning Electron Microscope with Energy Dispersive Spectra (SEM-EDS) techniques.

2.4. Slag and antimony characterization

The slag and metallic antimony were analyzed in an X-Ray Bruker D8 Focus with monochromatic Cu $K\alpha$ radiation working in $\theta/2\theta$ configuration. The following parameters were set for data collection: angular range from 10 to 70°, step size of 0.02°, and counting time of 2° min^{-1} . The slags were crushed in an agate mortar and sampled, while the metallic antimony samples were analyzed on the center zone. The antimony contents of both slag and metallic antimony were determined from analytical methods for atomic absorption spectrometry. Qualitative chemical analysis, morphology, and size of resulting slags were determined in an SEM Jeol 6300 and with the energy dispersive spectra analysis. A film deposit of Au-Pd on the surface of the slags was necessary to make them conductive. Backscattering electrons technique with 15 kV and 10 A was used for image production.

3. Thermodynamic modeling

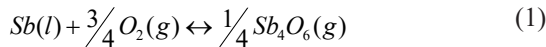
FactSage 7.3 [21] with the module Equilib was used to determine the concentration of the different



chemical species once they reach the chemical equilibrium state. The user provides the initial amount of chemical species, the temperature, and the pressure of the system (usually 1 atm), then the program calculates the most stable species with the Gibbs free energy minimization method.

3.1. Oxidation stage

The Equilib module and the FactPS, FToxide, and FSlead databases were used to estimate the antimony oxidation from a Pb-Sb alloy. As input data, a Pb-Sb alloy containing 2.1 wt% Sb (489.5 g Pb and 10.5 g Sb) which interacts with pure oxygen was considered. The effect of the oxygen amount on the phase formation was determined for a temperature of 750 °C and 1 atm. The oxidation reaction of antimony contained in the Pb-Sb melt was carried out according to reaction (1), where the Sb was volatilized to form the Sb_4O_6 (g) phase at high temperatures:

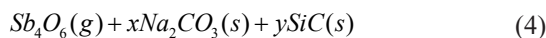
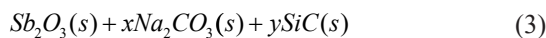


Afterward, the Sb_4O_6 (g) phase was deposited as the temperature decreased to form the antimony trioxide as follows:



3.2. Reduction stage

The computer simulation was carried out using the FactPS, Ftmisc, and the FToxid databases contained in the module Equilib. The effects of temperature and concentration of Na_2CO_3 and SiC in the recovery of antimony from antimony trioxide were theoretically estimated. The thermodynamic modeling considered the chemical composition of the antimony trioxide, sodium carbonate, and silicon carbide. The recovery process of antimony from Sb_2O_3 and Sb_4O_6 with Na_2CO_3 and SiC was established based on the following reactions:



Reaction (3) was carried out at lower temperatures while reaction (4) proceeded at higher temperatures, where according to G. Brooks et al. [22], the stable antimony oxide was the Sb_4O_6 as a gas phase. The reduction trials were carried out at 1000 °C, thus reaction (4) was expected to occur for the antimony reduction. Stability phase diagrams were obtained considering the effect of increasing the amounts of Na_2CO_3 and SiC to reduce the Sb_2O_3 . The initial data for simulating were 5 grams Sb_2O_3 , 2.5, 3.1, 3.7, and

4.3 grams Na_2CO_3 , which correspond to 30, 34, 38, and 42 wt.% Na_2CO_3 , respectively. The addition of SiC was considered till 1.2 grams. The modeling was carried out considering a closed system to 1 atmosphere of pressure and the temperature was held constant at 1000 °C.

4. Results and discussion

4.1. Pb-Sb alloy

Table 1 shows the chemical composition of the Pb-Sb alloy obtained from the molten terminals of lead-acid batteries.

Table 1. Chemical composition of the Pb-Sb alloy (wt.%)

Alloy	Sb	Cu	Fe	Ag	As	Bi	Pb
Pb-Sb	2.099	0.013	0.098	0.005	0.07	0.002	Balance

The concentration of antimony in lead-acid batteries has been declined in recent years due to advanced technology and the use of Ca, Al, and Sn alloys as a replacement [10]. As can be observed from Table 1 after lead, the major components in the alloys were antimony, followed by iron and arsenic with 0.098 and 0.070 wt.%, respectively. It was observed that arsenic and antimony existed in the terminals of lead-acid batteries like in other lead by-products. It was expected that arsenic and antimony would be volatilized during the oxygen injection as As_2O_3 and Sb_2O_3 .

4.2. Oxidation stage

After selective oxidation, the formed oxide (white powder) was manually collected from the gas exhaust, however, a higher quantity of antimony trioxide was found on the inner side of the lid. Figure 3a shows the stainless-steel lid during the oxygen injection and Figure 3b shows the antimony trioxide recovering from the inner side of the lid. The volatiles were cooled in colder regions of the inner chamber and deposited over them before they were collected into a water-cooled condenser.

The residual lead-rich alloy and the antimony trioxide in powder form were picked up, weighed, and analyzed by atomic absorption. Table 2 shows the chemical composition, the mass of the alloy, and the

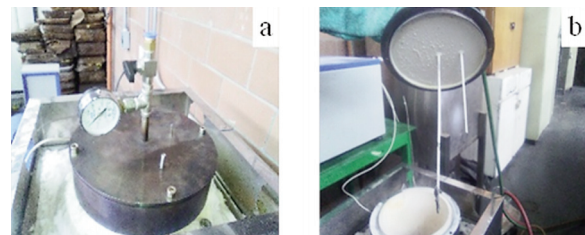


Figure 3. Experimental array for the oxidation stage, a) stainless steel lid and b) antimony trioxide deposited on the inner side of the lid

volatilized antimony recovered.

Table 2. Chemical composition of the Pb-Sb alloy (wt.%)

Product	Mass (g)	Sb	Cu	Fe	Ag	As	Bi	Pb
Pb	484.72	0.23	0.005	0.085	0.001	0.048	0.002	Balance
Sb oxide	9.49	80.14	0.002	0.002	0.001	0.089	0.001	0.27

The recovery of antimony as antimony trioxide was near to 78 wt.%. A Considerable amount of As and Fe remained in the lead-rich alloy. It has been reported that As is easy to volatilize as As_2O_3 reaching a volatilization rate of 93 wt.% in 120 min at 460 °C while the Sb_2O_3 also reaches 95 wt.% in 140 min at 600 °C [23, 24].

The antimony trioxide produced from the selective oxidation was analyzed by the atomic absorption and X-ray powder diffraction. The results were compared with Sb_2O_3 commercial-grade reagent. Figure 4 shows the X-ray diffraction patterns for the Sb_2O_3 produced in the oxidation stage and the commercial chemical reagent.

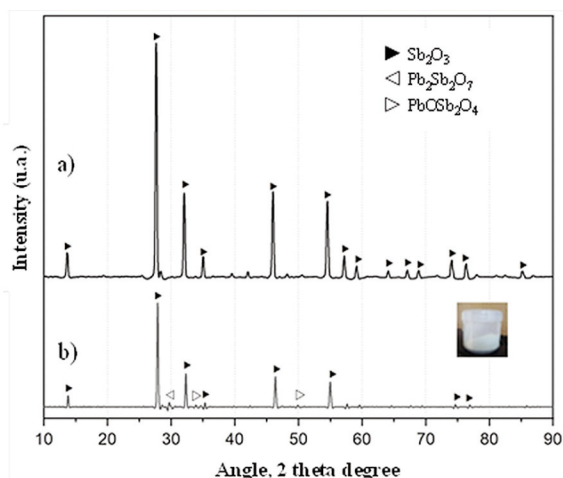


Figure 4. X-ray diffraction patterns of the antimony trioxide for a) commercial reagent, and b) selective oxidation

Figure 4 shows that the antimony trioxide produced in the selective oxidation contained as a major component the senarmontite phase (Sb_2O_3) with very lower amounts of bindeimita ($Pb_2Sb_2O_7$), and a Pb-Sb oxide ($PbOSb_2O_4$) while the commercial reagent showed only the senarmontite phase. The antimony trioxide produced reached 96 wt.% of purity. Taking as reference the purity of antimony trioxide from the selective oxidation from lead-antimony alloy and the few quantities of antimony trioxide produced, the experimental part concerning the reduction stage was conducted with analytical grade antimony trioxide.

4.3. Reduction stage

Tables 3 and 4 show the chemical composition by atomic absorption spectroscopy of the metallic antimony and the slags formed, respectively, obtained by the trioxide antimony reduction process to different amounts of Na_2CO_3 . Tables 3 and 4 also show the mass of the products formed.

Table 3. Chemical composition of the antimony metallic to different Na_2CO_3 additions (wt.%)

Na_2CO_3 (wt.%)	Sb (g)	Chemical composition (wt.%)						
		Sb	Si	Na	Pb	Bi	Cu	Fe
30	3.14	98.62	0.31	1.05	0.016	0.0006	0.0005	0.0002
34	3.72	99.69	0.19	0.12	0.0012	0.0006	0.0008	0.0003
38	3.29	98.62	0.29	1.08	0.0062	0.0012	0.0003	0.0005
42	3.14	98.71	0.31	0.98	0.0013	0.0009	0.0003	0.0005

Table 4. Chemical composition of the slags to different Na_2CO_3 additions (wt.%)

Na_2CO_3 (wt.%)	Slag (g)	Chemical composition (wt.%)		
		Sb	Si	Na
30	2.85	2.34	15.58	22.8
34	2.78	1.71	20.22	23.9
38	3.46	6.63	15.25	24.1
42	3.96	16.53	15.55	24.24

The chemical composition of the antimony metallic showed that the main impurities in the antimony metallic button were silicon and sodium. The highest recovery (90%) and grade (99.69%) of the antimony metallic button were obtained in a single-step process for the addition of 34 wt.% Na_2CO_3 . In all cases, reached grade for metallic antimony buttons was very close to the commercial antimony grade (99.65%). The slags obtained from the reduction process of trioxide antimony to different Na_2CO_3 amounts with SiC at 1000 °C showed high Silicon and Sodium contents, above 15.25 and 22.80 wt.%, respectively. Antimony concentration in the slag reached values between 1.71 and 16.53 wt.%. Its presence confirmed the reaction between antimony oxide and the added reactants SiC and Na_2CO_3 to produce metallic antimony, where the carbon from the SiC and the Na_2CO_3 acted as reducing agents of trioxide antimony, while Silicon and Sodium were in the slag phase, which may form mainly sodium and antimony silicates. It has been reported [17] that the Sb_2O_3 content in SiO_2 shows a stable tendency within the temperature range of 900 to 1200 °C, therefore, the Sb-containing phase primarily changed from the solid solution phase to the Sb-silicate phase.

Figures 5 and 6 show the antimony recovery as a

function of the different amounts of Na_2CO_3 added (30, 34, 38, and 40 wt.%), keeping the SiC constant of 0.95 g at 1000 °C for the antimony metallic button and the slag, respectively.

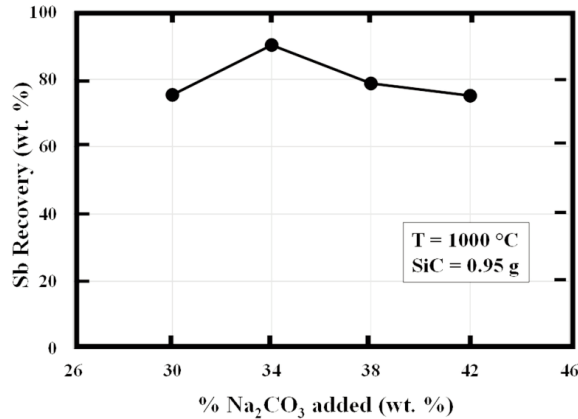


Figure 5. Antimony recovery from trioxide antimony reduction with SiC and different amounts of Na_2CO_3 to 1000 °C

It is observed from Figure 5 that the recovery rates of the metallic antimony were in the range from 75.12 to 90.16 wt.%. These results were in the range reported in the traditional pyrometallurgical antimony route [3,10]. The antimony grade was between 98.62 wt% and 99.69 wt%. An increment of the metallic antimony recovery was observed when the sodium carbonate increased from 30 to 34 wt%, reaching the highest antimony recovery value (90.16 wt%) for the Na_2CO_3 addition of 34 wt%. As expected, for the same Na_2CO_3 additions, the lowest antimony contents

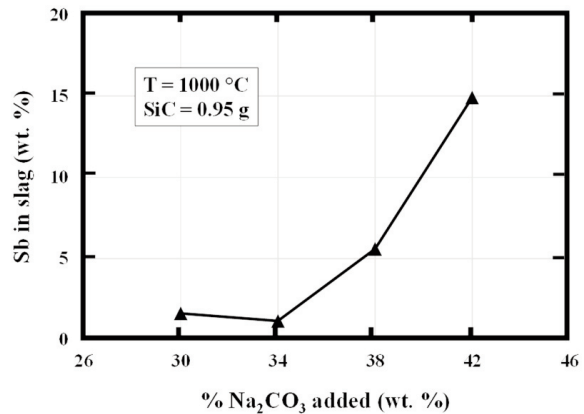


Figure 6. Antimony content in the slag obtained from the trioxide antimony reduction with SiC and different amounts of Na_2CO_3 to 1000 °C

were obtained in the slag. However, as the sodium carbonate content increased from 34 to 42 wt. %, the recovery of metallic antimony decreased obtaining an increase of the slag mass and the antimony content, which reached a value up to 14.92 wt.%.

A difference in the brightness of the obtained antimony metallic button was evident, low-grade antimony buttons showed an opaque luster while high-grade buttons showed a shining metallic. The luster differences on the antimony button occurred due to a residual slag film deposited on the metallic antimony formed after cooling and phase separation. The metallic antimony button obtained for the addition of 34 wt.% Na_2CO_3 was analyzed with the SEM-EDS technique and Figure 7 shows a micrograph of the metallic sample with its X-ray

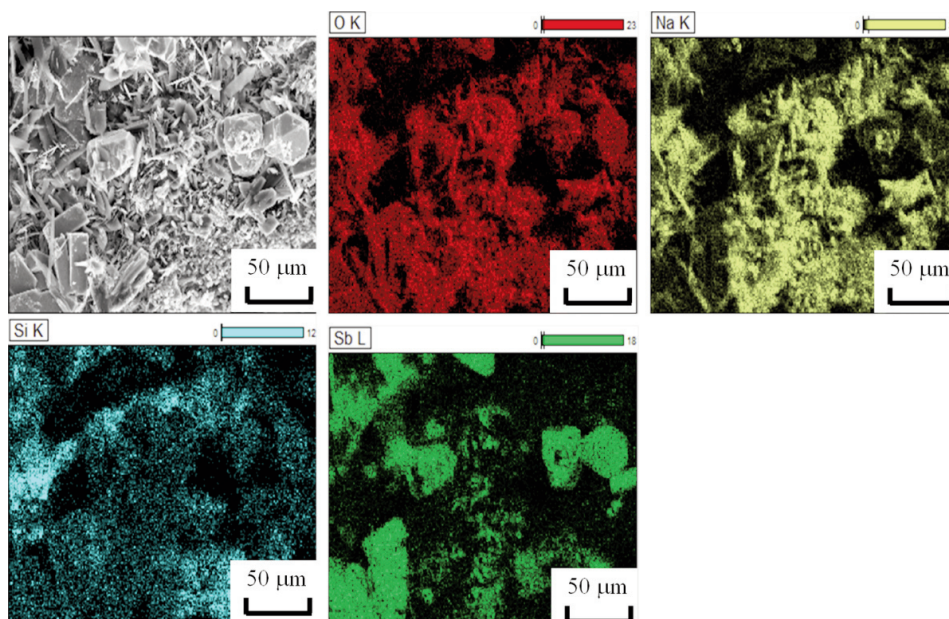


Figure 7. SEM micrograph and X-ray mapping images of metallic antimony obtained to 34 wt.% Na_2CO_3

mapping images for Sb, Na, Si, and O. The micrograph showed the presence of particles with different morphology. Some type-whiskers particles constituted of mainly by Na, Si, and O with the same distribution were observed. On the other hand, antimony was concentrated in particles with rhombohedral and tetrahedral forms, as well as columnar and elongated crystals. A low concentration of antimony small particles was distributed all over the analyzed surface.

Figures 8a and 8b show the micrographs and their microanalysis of the whiskers and the elongated particles showed in Figure 7. Whiskers particles were

mainly constituted of high contents of Na, Si, and O (Figure 8a), while the elongated morphologies particles corresponded to the metallic antimony button (Figure 8b), which were notably bigger than whiskers particles of the residual slag film.

The SEM and EDS patterns results of the slag obtained for antimony recovery from Pb-Sb alloy reduction trials with SiC are shown in Figures 9a and 9b for the Na_2CO_3 additions of and 34 and 38 wt.%, respectively. The microanalysis showed that the amount of antimony in the slag increased when the amount of sodium carbonate was increased from 34 to 38 wt.%. The microanalysis showed in both cases the

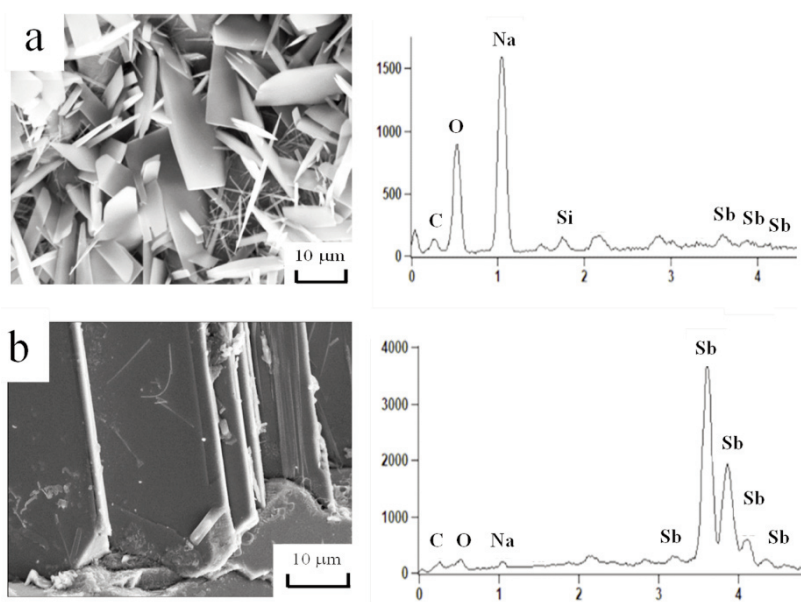


Figure 8. SEM micrographs and microanalysis of the metallic antimony obtained for the Na_2CO_3 addition of 34 wt.% for a) whiskers particles and b) elongated crystals

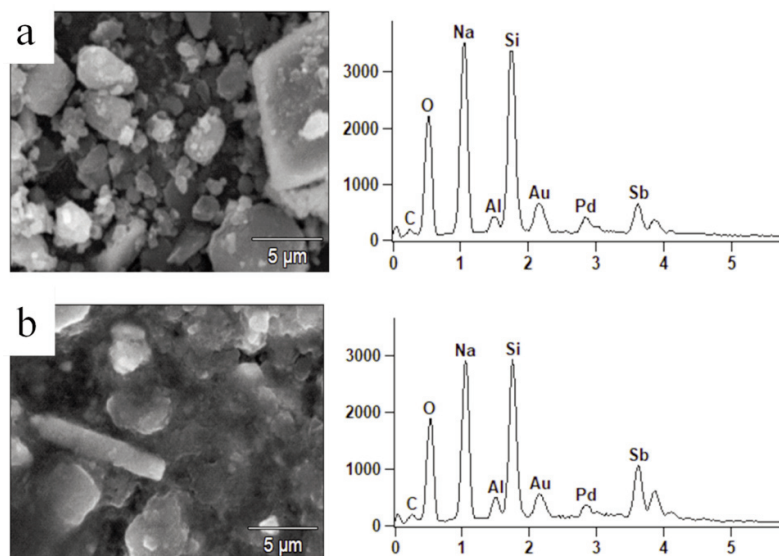


Figure 9. SEM micrographs and microanalysis of the slags obtained to (a) 34 wt.% Na_2CO_3 and (b) 38 wt.% Na_2CO_3

presence of silicon, sodium, and oxygen attributed to the raw materials used in the reduction trials. More defined morphologies like crystals normally presented in silicates were observed in the slag obtained to the addition of 34 wt.% Na_2CO_3 , while the slag obtained to 38 wt.% Na_2CO_3 showed fewer crystalline particles, most of them with undefined morphology. The detection of gold and palladium occurred due to the Au-Pd film deposited on the slags to make them conductive.

The antimony metallic button and the slag obtained during the antimony trioxide reduction trials were characterized by the X-ray diffraction and results are observed in Figures 10 and 11, respectively. Figure 10 shows that the metallic antimony obtained to 30 and 34 wt.% Na_2CO_3 was mainly constituted of metallic antimony, and few amounts of unreacted Na_2CO_3 and SiO_2 appeared for the lowest Na_2CO_3 addition. When the amount of Na_2CO_3 was increased, antimony remained as the main phase, however, small amounts of the silicate $\text{Na}_2\text{Si}_2\text{O}_5$ and SiO_2 were detected to the Na_2CO_3 addition of 38 wt.%. For the highest Na_2CO_3 addition (42 wt.%), the antimony metallic contained the $\text{Na}_2\text{Si}_4\text{O}_9$ phase and unreacted Na_2CO_3 . The highest recovery and grade of metallic antimony were obtained to the Na_2CO_3 addition of 34 wt.%, which agreed with its X-ray diffraction pattern, where only the presence of metallic antimony was detected.

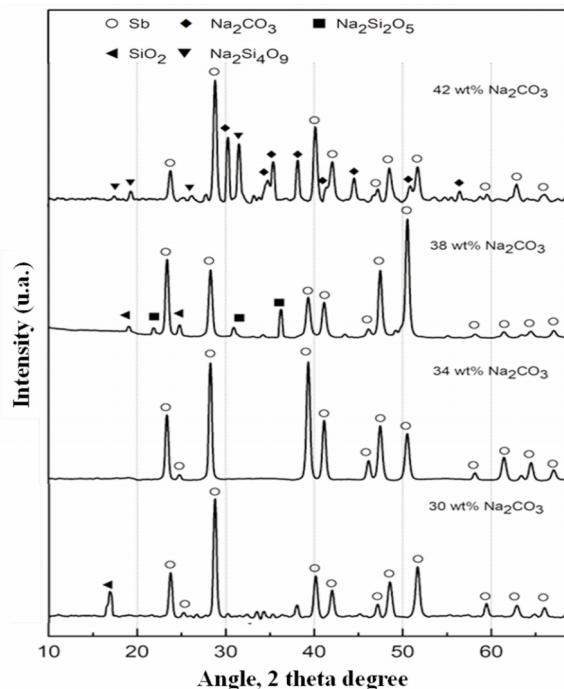


Figure 10. X-ray diffraction patterns of the metallic antimony samples obtained after trioxide reduction with 0.95 g SiC and 1000 °C to different Na_2CO_3 contents

Figure 11 shows the X-ray diffraction patterns of the slags obtained for the antimony trioxide reduction trials. The X-ray pattern obtained for the addition of 30 wt.% Na_2CO_3 showed the presence of Sb_2O_3 , Na_2CO_3 , SiO_2 , and C unreacted and the Na_2SiO_3 and hydrated Na_2CO_3 as compounds formed. It was evident for the Na_2CO_3 addition of 34 wt.% that the raw materials reacted to form mainly the Na_2SiO_3 and NaSb_3O_7 compounds. In addition, few amounts of Na_2CO_3 and C unreacted were also detected. For the higher Na_2CO_3 additions evaluated, an increase of the compounds formed such as sodium antimonates NaSb_3O_7 , $\text{Na}_2\text{Sb}_4\text{O}_7$, silicates such as Na_2SiO_3 , $\text{Na}_2\text{Si}_2\text{O}_5$ with C and unreacted Na_2CO_3 was evident. Because of the high volatility of trioxide antimony, it was observed in some slag samples their presence in few amounts. For the Na_2CO_3 addition of 38 wt.%, the main compounds were Na_2CO_3 and hydrated Na_2CO_3 , the amount of the Na_2SiO_3 compound decreased while the $\text{Na}_2\text{Sb}_4\text{O}_7$ was formed. The slag obtained for the highest Na_2CO_3 addition showed an increase in the $\text{Na}_2\text{Sb}_4\text{O}_7$ compound and the appearance of the $\text{Na}_2\text{Si}_2\text{O}_5$ compound. Besides, the $\text{Na}_2\text{C}_2\text{O}_4$ compound was detected which corresponded to acetylene diolate. It is already known that alkali metals react with carbon monoxide [18, 25], in this case, Na_2CO_3 content allowed the sodium acetylene diolate formation during the thermal decomposition of the carbonates in the charge. The carbonate-based slags (Na_2CO_3), also known as soda slags, were easily leachable and hydrated as was observed in Figure 11, however, the silica addition allowed the formation of more stable slags [9]. It was observed for the addition of 34 wt.% Na_2CO_3 , that the Na_2SiO_3 compound

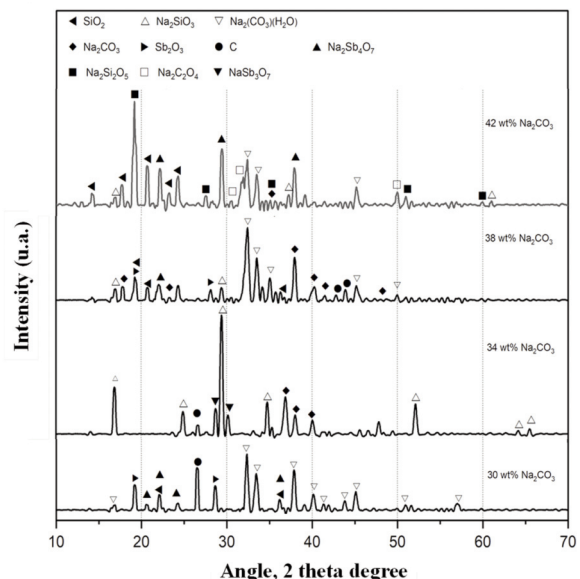


Figure 11. X-ray diffraction patterns for slags obtained after trioxide reduction with 0.95 g SiC and 1000 °C to different Na_2CO_3 contents

formed showed high stability to weather degradation. Experimentally, few and small hardly noticeable antimony droplets were found trapped in the slag phase, which was not taken into account in the antimony recovery rates and the slag characterization.

4.4. Thermodynamic modeling

4.4.1. Oxidation stage

Figure 12a, b shows a stability diagram that represents the oxidation stage of the antimony contained in a Pb-Sb alloy. Figure 12a shows the elements considered in the oxidation and the compounds formed at equilibrium when oxygen reacted with 500 grams of a lead-antimony melted alloy at 750 °C. Formation of Sb_4O_6 (g) started immediately with the presence of O_2 , its amount increased steadily as the content of antimony in the lead-antimony alloy decreased, because antimony had a higher affinity with oxygen than lead, it reacted with oxygen to form Sb_4O_6 (g) easily. Lead oxide was formed until antimony was almost completely oxidized. As the lead oxide increased, the amount of melted lead decreased. Figure 12b shows a close-up image of selective oxidation of antimony. According to the stability diagram, to separate almost all antimony as Sb_4O_6 (g) from 500 g lead-antimony (2.1% by weight antimony) alloy at 750°C about 1.7 grams of oxygen were needed, which represented at standard conditions of pressure and temperature 0.14 liters for each gram of antimony in the alloy. Under those conditions, the expected quantity that could be produced of Sb_4O_6 (g) was about 9.6 grams.

The Sb_4O_6 (g) formation occurred easily due to its high vapor pressure when oxidation reaction was carried out (Eq. 1), then, Sb_2O_3 (s) was deposited when the Sb_4O_6 (g) was cooled. Experimentally, 9.49 g were obtained which reasonably matched with the expected 9.7 g with the predicted results in FactSage 7.3.

4.4.2. Reduction stage

Figures 13a and 13b show the stability diagram calculated in FactSage 7.3 considering a mass and a molar charge for reaction (3), respectively. It is observed that as the reagent SiC was added up to 1.2 grams, the Sb_4O_6 (g), which was thermodynamically the stable antimony oxide at 1000 °C, decreased, while Sb (l) phase increased. Because of its volatility, a quantity of reduced antimony in the gas phase was formed. Antimony volatilization also happens in the traditional antimony production mainly from sulfides concentrated ores by pyrometallurgical route, where antimony losses by volatilization could reach values up to 20 wt.% or even higher [26, 27]. To 1000 °C, the Na_2CO_3 was thermally dissociated to form Na_2O (s) and CO_2 (g), the Na_2O reacted with Si from the SiC to form slag with two different types of silicates $\text{Na}_6\text{Si}_2\text{O}_7$ and Na_2SiO_3 , both in a liquid phase, while the CO_2 (g) was later reduced with higher amounts of SiC added to form CO (g). It was expected that during the reduction stage, the produced CO (g), and the C from the SiC would aid in the antimony reduction. The stability of each silicate depended on the concentration of SiC, even $\text{Na}_6\text{Si}_2\text{O}_7$, and Na_2SiO_3 partially coexisted in the range from 0.1 to 0.2 and from 0.6 to 1.2 g SiC, respectively. According to FactSage 7.3 equilibrium results, the highest amount of antimony was produced when 0.6 g of SiC was added to 5 g Sb_2O_3 reaching up to 3.9 g of liquid antimony and 0.2 g of volatilized antimony. For the experimental conditions evaluated, the reduction results reasonably matched with the predicted results. As the SiC content was increased from 0.6 to 1.2 grams, the content of formed silicates $\text{Na}_6\text{Si}_2\text{O}_7$ and Na_2SiO_3 was increased, while melted Na_2CO_3 reacted totally. Over this content interval of SiC, the volatilized antimony quantity increased slightly with the corresponding diminution of the liquid antimony.

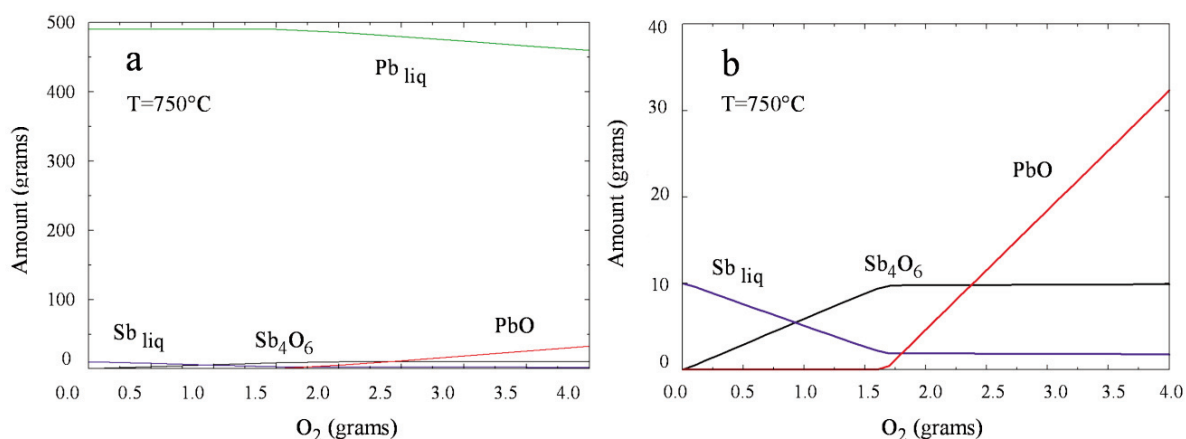


Figure 12. a) Compounds produced at equilibrium when 500 g of lead-antimony (2.1 wt.% Sb) alloy reacts with oxygen to 750 °C and b) close-up image of antimony oxidation

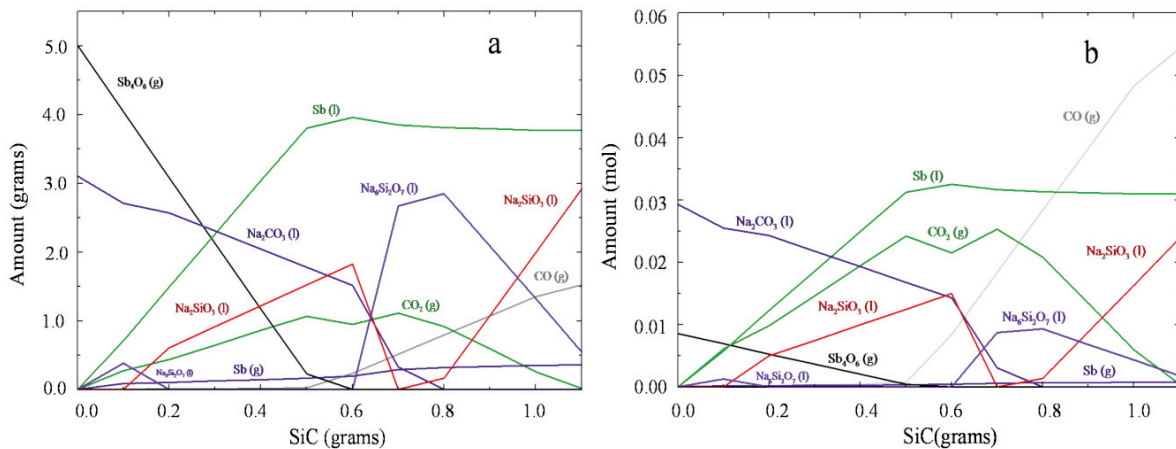


Figure 13. Stability phase diagram for the $Sb_2O_3(s)+x Na_2CO_3(s)+y SiC(s)$ system evaluated to 34 wt% Na_2CO_3 to 1000 °C for a) mass charge and b) molar charge

The silicate phases $Na_6Si_2O_7$ and Na_2SiO_3 experimentally formed were successfully predicted by the Factsage software, however, the phases formed containing antimony ($NaSb_3O_7$ and $Na_2Sb_4O_7$) were not predicted because the used databases did not contain them. However, the thermodynamic modeling allowed more precise understanding of the experimental results of the pyrometallurgical process involved in this study.

The conventional reduction-smelting of lead-acid batteries is conducted in reverberatory or rotary furnaces. A crude lead-antimony alloy and an antimony-rich slag are obtained from the melt of the secondary materials. Antimony oxide in the slag is subsequently reduced with carbon contained in coke to produce antimony metal [1]. In this work, mixtures of Na_2CO_3 -SiC were used to reduce the antimony trioxide in laboratory-level tests obtaining good antimony recovery and grade. However, it must be noted that SiO_2 and C have been successfully used instead of SiC in the recovery of antimony from antimonial dust [11] which may represent the cheapest option if the temperature and viscosity of the melt are controlled.

5. Conclusions

Antimony was recovered from recycled terminals from spent lead acid-batteries by a pyrometallurgical process which comprised an oxidation stage to produce $Sb_4O_6(g)$ that was cooled and recovered as $Sb_2O_3(s)$ and further reduced with a mixture of SiC and Na_2CO_3 at 1000 °C. The results are summarized as follows:

1. The recycled terminals from spent lead-acid batteries allowed to obtain a Pb-2 wt% Sb alloy with arsenic and iron as main impurities.
2. High purity Sb_2O_3 (96 wt%) was obtained during the oxidation stage by the oxygen injection of

2 L min^{-1} O_2 , for 0.5 min at 750 °C. The recovery was 78 wt%.

3. It was possible to carry out the antimony reduction from Sb_2O_3 using SiC- Na_2CO_3 mixtures at 1000 °C.

4. The highest metallic antimony recovering (90 wt%) and grade (99.69 wt%) together with the lowest slag amount containing the lowest Sb content was obtained for the Na_2CO_3 addition of 34 wt%.

5. During the Sb reduction, the addition of 34 wt% Na_2CO_3 promoted mainly the Na_2SiO_3 compound formation with small amounts of $NaSb_3O_7$, however, when the amount of sodium carbonate increased, the $Na_2Sb_4O_7$ compound was formed, increasing the Sb content in the slag.

6. The thermodynamic modeling reasonably matched with the experimental results for the oxidation and reduction stages involved as well in the compounds predictions.

Acknowledgments

The authors wish to thank the Institutions CONACyT, SNI, COFAA, and SIP-Instituto Politécnico Nacional for their permanent assistance to the Process Metallurgy Group at ESQIE-Metallurgy and Materials Department.

Author Contributions

Conceptualization: J.C. Jiménez-Lugos, R.G. Sánchez-Alvarado and A. Cruz-Ramírez; Investigation: J.C. Jiménez-Lugos, A. Hernández-Ramírez and J.A. Romero-Serrano; Methodology: J.C. Jiménez-Lugos, A. Hernández-Ramírez and R.G. Sánchez-Alvarado; Supervision: A. Cruz-Ramírez and R.G. Sánchez-Alvarado; Visualization: R.G. Sánchez-Alvarado, J.C. Jiménez-Lugos and A. Cruz-Ramírez. Writing-original draft: R.G. Sánchez-Alvarado and



J.C. Jiménez-Lugos; Writing - review and editing: A. Cruz-Ramírez and R.G. Sánchez-Alvarado; Funding acquisition: A. Cruz-Ramírez and R.G. Sánchez-Alvarado. All authors have read and agreed to the published version of the manuscript.

Data Availability Statement

No additional data.

Conflicts of Interest

The authors declare no conflict of interest.

References

- [1] G. Gunn, Critical Metals Handbook, John Wiley & Sons, Oxford, UK, 2014, p70.
- [2] C. Zhang, C. Catlow, The mechanism of propene oxidation to acrolein in iron antimony oxide, *Journal of Catalysis*, 259 (1) (2008) 17-25. <https://doi.org/10.1016/j.jcat.2008.06.027>.
- [3] C. Anderson, The metallurgy of antimony, *Chemie der Erde*, 72 (S4) (2012) 3-8. <https://doi.org/10.1016/j.chemer.2012.04.001>.
- [4] T. Liu, K. Qiu, Removing antimony from waste lead storage batteries alloy by vacuum displacement reaction technology, *Journal of Hazardous Materials*, 347 (2018) 334-340. <https://doi.org/10.1016/j.jhazmat.2018.01.017>.
- [5] R. Multani, T. Feldmann, G. Demopoulos, Antimony in the metallurgical industry: A review of its chemistry and environmental stabilization options, *Hydrometallurgy*, 164 (2016) 141-153. <https://doi.org/10.1016/j.hydromet.2016.06.014>.
- [6] D. Lin, K. Qiu, Removal of arsenic and antimony from anode slime by vacuum dynamic flash reduction, *Environmental Science and Technology*, 45 (8) (2011) 3361-3366. <https://doi.org/10.1021/es103424u>.
- [7] C. Anderson, Hydrometallurgically treating antimony-bearing industrial wastes, *The Journal of The Minerals, Metals & Materials Society (TMS)*, 53 (2001) 18-20. <https://doi.org/10.1007/s11837-001-0156-y>.
- [8] V. Krenev, N. Dergacheva, S. Fomichev, Antimony: Resources, application fields, and world market, *Theoretical Foundations of Chemical Engineering*, 49 (2015) 769-772. <https://doi.org/10.1134/S0040579515050115>.
- [9] T. Ellis, A. Mirza, The refining of secondary lead for use in advanced lead-acid batteries, *Journal of Power Sources*, 195 (14) (2010) 4525-4529. <https://doi.org/10.1016/j.jpowsour.2009.12.118>.
- [10] D. Dupont, S. Arnout, P. Jones, K. Binnemans, Antimony recovery from end-of-life products and industrial process residues: A critical review, *Journal of Sustainable Metallurgy*, 2 (2016) 79-103. <https://doi.org/10.1007/s40831-016-0043-y>.
- [11] W. Liu, T. Yang, D. Zhang, L. Chen, Y. Liu, A new pyrometallurgical process for producing antimony white from by-product of lead smelting, *The Journal of The Minerals, Metals & Materials Society (TMS)*, 66 (9) (2014) 1694-1700. <https://doi.org/10.1007/s11837-014-1026-8>
- [12] D. Zhong, L. Li, Ch. Tan, Recovery of antimony from antimony-bearing dusts through reduction roasting process under CO-CO₂ mixture gas atmosphere after firstly oxidation roasted, *Journal of Central South University*, 25 (2018) 1904-1913. <https://doi.org/10.1007/s11771-018-3880-y>
- [13] B. Padilla, L. Chambi, M. Ruiz, Antimony production by carbothermic reduction of stibnite in the presence of lime, *Journal of Mining and Metallurgy, Section B-Metallurgy*, 50 (1) (2014) 5-13. <https://doi.org/10.2298/JMMB130604003P>.
- [14] J. Yang, Ch. Tang, Y. Chen, M. Tang, Separation of antimony from a stibnite concentrate through a low-temperature smelting process to eliminate SO₂ emission, *Metallurgical and Materials Transactions B*, 42B (2011) 30-36. <https://doi.org/10.1007/s11663-010-9453-6>.
- [15] B. Friederich, A. Arnold, F. Toubartz, Proceedings of European Metallurgical Conference, September 2011, Friedrichshafen, Germany, 2011, p. 295-317.
- [16] J. Xu, J. Gao, L. Kong, B. Xu, B. Yang, D. Liu, Isobaric vapor-liquid equilibria of ternary lead-tin-antimony alloy system at 2 Pa, *Journal of Mining and Metallurgy, Section B-Metallurgy*, 56 (3) (2020) 327-335. <https://doi.org/10.2298/JMMB190529026X>.
- [17] Z. Zhang, H. Nie, K. Yan, Sb distribution in the phases of SiO₂ saturated Sb-Fe-O-SiO₂-CaO system in air, *Journal of Mining and Metallurgy, Section B-Metallurgy*, 57 (1) (2021) 13-19. <https://doi.org/10.2298/JMMB200406030Z>.
- [18] J. Barragan, C. Ponce, J. Alemán, A. Peregrina, F. Gómez, and E. Larios, Copper and antimony recovery from electronic waste by hydrometallurgical and electrochemical techniques, *ACS Omega*, 5 (2020) 12355-12363. <https://doi.org/10.1021/acsomega.0c01100>.
- [19] J. Barragan, J. Alemán, A. Peregrina, M. Sánchez, E. Rivero, E. Larios, Leaching of metals from e-waste: From its thermodynamic analysis and design to its implementation and optimization, *ACS Omega*, 6 (2021) 12063-12071. <https://doi.org/10.1021/acsomega.1c00724>.
- [20] A. Sánchez, V. Gutiérrez, A. Cruz, R. Sánchez, Lead production from recycled paste of lead acid batteries with SiC-Na₂CO₃, *Russian Journal of Non-Ferrous Metals*, 57 (4) (2016) 316-324. <https://doi.org/10.3103/S1067821216040118>.
- [21] C. Bale, A. Pelton, W. Thompson. Facility for the Analysis of Chemical Thermodynamics (FactSage, v. 7.3), User's Manual, (2018).
- [22] G. Brooks, W. Rankin, N. Gray, Thermal separation of arsenic and antimony oxides, *Metallurgical and Materials Transactions B*, 25B (1994) 873-884. <https://doi.org/10.1007/BF02662769>.
- [23] G. Brooks, Ph. D. Thesis, The University of Melbourne, Melbourne, Australia, 1993.
- [24] A. Aracena, O. Jerez, C. Antonucci, Senarmontite volatilization kinetics in nitrogen atmosphere at roasting/melting temperatures, *Transactions of Nonferrous Metals Society of China*, 26 (1) (2016) 294-300. [https://doi.org/10.1016/S1003-6326\(16\)64117-1](https://doi.org/10.1016/S1003-6326(16)64117-1).
- [25] R. West, Oxocarbons, Academic Press, New York, USA, 1980, p. 3.



- [26] Y. Hua, Y. Yang, F. Zhu, Volatilization kinetics of Sb₂S₃ in steam atmosphere, Journal of Materials Science and Technology, 19 (6) (2003), 619-622.
- [27] W. Qin, H. Luo, W. Liu, Y. Zheng, K. Yang, J. Han,

Mechanism of stibnite volatilization at high temperature, Journal of Central South University, 22 (2015) 868-873. <https://doi.org/10.1007/s11771-015-2595-6>.

ISKORIŠĆENJE ANTIMONA IZ RECIKLIRANIH TERMINALA OLOVNO-KISELIH BATERIJA KOJE SADRŽE Na₂CO₃ I SiC NAKON FORMIRANJA Sb₂O₃

J.C. Jiménez-Lugos ^a, R.G. Sánchez-Alvarado ^a, A. Cruz-Ramírez ^{a,*},
J.A. Romero-Serrano ^a, A. Hernández-Ramírez ^a, J.E. Rivera-Salinas ^b

^a Nacionalni politehnički institut - ESQIE, Odsek za metalurško inženjerstvo i materijale, Meksiko Siti, Meksiko

^b Centar za istraživanje primenjene hemije - CIQA, Odsek za preradu plastike, Saltijo, Koavila, Meksiko

Apstrakt

Terminali dobijeni iz istrošenih olovno-kiselih baterija u Meksiku sadrže oko 2 wt% Sb. Terminali su rastopljeni u električnoj peći, a zatim je injektiran kiseonik na 750 °C sa brzinom protoka gasa od 2 L/min da bi se dobio Sb₂O₃ visoke čistoće. Dobijeni antimon trioksid je tretiran mešavinom Na₂CO₃-SiC na 1000 °C da bi se dobio metalni antimon. Antimon trioksid je redukovan u prisustvu C koji se nalazi u reagensima, dok su silicijum i natrijum formirali fazu šljake. Količine Sb₂O₃ i SiC su bile konstantne, dok je procenjena količina Na₂CO₃ iznosila između 30 i 42 wt%. Dobijeni antimon i šljaka su ispitani rendgenskom difrakcijom i SEM-EDS tehnikama. Dodavanje 34 wt% Na₂CO₃ doprinelo je iskorišćenju antimona od 90,16 wt% (čistoće 99,57 wt%) i najmanjeg gubitka antimona u šljaci (2 wt%). Pored toga, jedinjenja Na₂SiO₃ i Na₂Si₂O₇ nastala u šljaci ukazuju na stabilniju šljaku. Sadržaj Na₂CO₃ veći od 38 wt% smanjio je iskorišćenje antimona pošto je jedinjenje Na₂Sb₄O₇ formirano u šljaci. Proces oksidacije i redukcije je modelovan u FactSage 7.3 softveru radi boljeg razumevanja uticaja dodavanja Na₂CO₃ i SiC na stopu iskorišćenja antimona i jedinjenja koja se formiraju u šljaci.

Ključne reči: Antimon; Redukcija; Šljaka; Baterije; Termodinamika

